

The design, synthesis and fluorescent sensing applications of a thermo-sensitive Zn-MOF



Ensheng Zhang^{a,*}, Long Jiang^b, Ruijiang Lv^c, Shiyang Li^a, Rongmei Kong^a, Lian Xia^a, Ping Ju^{a,**}, Fengli Qu^{a,***}

^a College of Chemistry and Chemical Engineering, Qufu Normal University, Qufu, Shandong, 273165, PR China

^b Instrumental Analysis & Research Center, Sun Yat-Sen University, Guangzhou 510275, PR China

^c Shandong LuTai Holding Group Co.,Ltd, Shandong, 273165, PR China

ARTICLE INFO

Keywords:

Zn-MOF
Thermo-sensitive material
Fluorescent probe

ABSTRACT

A novel fluorescent Zn-MOF $[\text{Zn}(\text{cca})_{0.5}(\text{TPB})_{0.5}(\text{H}_2\text{O})_2] \cdot (\text{NO}_3) \cdot (\text{H}_2\text{O})_2$ (complex 1) and its multipurpose sensing applications have been revealed. By embedding 1, 2, 4, 5-tetra(4-pyridyl)benzene (TPB, the AIE ligand) into the framework of complex 1, a fluorescent Zn-MOF with good thermo-sensitive properties in a wide temperature range (30 °C–200 °C) was obtained. Remarkable fluorescent emission was observed for complex 1 both in solid and solvents. An emission red shift (30 nm) of complex 1 after dispersed in H₂O compared with that in other solvents were recorded, which could be used in the distinguishing H₂O from other solvents. PXRD tests revealed the good stability of complex 1 in both organic and inorganic solvents. Stable suspension was obtained after dispersed complex 1 in deionized water and used in the fluorescent detection acetone and metal ions in water. Real-time fluorescent quenching sensing of acetone in water was accomplished with an experimental detection limit as 0.03% (vol. %) based on the inner filter effect (IFE). Interestingly, significant fluorescent enhancement of complex 1-H₂O suspensions was detected after mixed with Al³⁺, while, obvious fluorescent quenching was recorded after treatment with Cu²⁺. In addition, the experimental detection limits for Al³⁺ and Cu²⁺ were 1.33 μM and 0.67 μM, respectively.

1. Introduction

Luminescent metal-organic frameworks (LMOFs) are promising candidates to construct fluorescent sensors owing to their intriguing framework architecture, interesting topology and multipurpose optical properties [1–4]. To date, various fluorescent MOF sensors were fabricated for the detection of metal ions [5–7], nitroaromatic explosives [8–10], VOCs [11–14] and bioactive molecules [15–17] et al. Besides, by taking advantage of MOFs, multi-functional materials for temperature [18], humidity [19,20], mechanical pressure [18,21] and battery-type electrodes [22–25] have been rationally designed and constructed. Temperature, as one of the most important physical parameter in both industrial process control and biochemical processes, deserve more concerns. According to previous studies, most of the revealed temperature responsive MOFs were mainly fabricated with flexible frameworks [26–28] or lanthanide ions based coordination polymers [29–34]. The

mechanism for these fluorescent thermometers could be concluded as framework transformations or lanthanide ions based thermal responsiveness. As is well-known, circumstance temperature change greatly affect the intramolecular motion of aggregation-induced emission (AIE) molecules which will change the radiative/nonradiative decay rate and lead to the fluorescent intensity variation [35–37]. Thus, temperature responsive MOFs with high thermo-sensitivity and wide temperature response range might be fabricated with AIE organic ligands.

1, 2, 4, 5-Tetra (4-pyridyl)benzene (TPB) is a tetradentate AIE ligand which possess the X configuration [38,39]. Due to the good coordination effect of pyridine rings, TPB could be used as a promising candidate ligand for MOF construction. However, only a few MOFs that constructed with TPB ligand have been reported thus far [40–45]. Meanwhile, due to the lone pair electrons served as the coordination sites, the rotation of pyridine rings will not destroy the framework of MOFs. Thus, high stable and sensitive thermal-response LMOFs with interesting porous structure and intriguing

* Corresponding author.

** Corresponding author.

*** Corresponding author.

E-mail addresses: sdzes2006@163.com (E. Zhang), xiangjianhuan110@163.com (P. Ju), fengliquhn@hotmail.com (F. Qu).

<https://doi.org/10.1016/j.jssc.2021.122476>

Received 18 June 2021; Received in revised form 16 July 2021; Accepted 27 July 2021

Available online 31 July 2021

0022-4596/© 2021 Elsevier Inc. All rights reserved.

sensing applications might be fabricated with TPB ligands. Herein, we reveal the design, synthesis, thermal sensitive property and fluorescent sensing application of $[\text{Zn}(\text{cca})_{0.5}(\text{TPB})_{0.5}(\text{H}_2\text{O})_2] \cdot (\text{NO}_3) \cdot (\text{H}_2\text{O})_2$ (complex 1).

By embedding TPB into the framework as the ligand, a fluorescent MOF (complex 1) has been constructed. Complex 1 possess a 3D cationic framework with 1D channel which filled with nitrate ions, coordinated and lattice water molecules. Thermo-sensitive fluorescent quenching was observed in a wide temperature range, revealing the good temperature sensing application of complex 1. Besides, PXRD tests proved the good stability of complex 1 in various solvents such as water and acetone. Moreover, strong fluorescent emission was observed for complex 1 both in solid state and in solvents. In addition, stable suspensions were obtained by dispersing complex 1 in deionized water and used in the fluorescent sensing of acetone, Al^{3+} and Cu^{2+} in water with good selectivity and sensitivity.

2. Experimental sections

2.1 Reagents and instruments

4-Carboxycinnamic acid (H_2cca), TPB and other reagents were bought from commercial reagent companies with analytical purity. X-ray diffraction (XRD) patterns were performed using a Panalytical X-ray Diffractometer. A Vario EL elemental analyzer was used for C, H and N analyses. The IR spectra were obtained as KBr disks on a Nicolet NEXUS 470-FTIR Spectrophotometer. The thermogravimetric analyses (TGA) were recorded using a Netzsch TG-209 Thermogravimetry Analyzer. Fluorescent spectra were tested by using an Agilent Cary Eclipse fluorescence spectrophotometer and a HITACHI fluorescence spectrophotometer (F4600).

2.2. Synthesis of $[\text{Zn}(\text{cca})_{0.5}(\text{TPB})_{0.5}(\text{H}_2\text{O})_2] \cdot (\text{NO}_3) \cdot (\text{H}_2\text{O})_2$ (complex 1)

To a glass scintillation vial (20 mL) was added $\text{Zn}(\text{NO}_3)_2 \cdot 6\text{H}_2\text{O}$ (0.015 g, 0.05 mmol), H_2cca (0.006 g, 0.03 mmol), TPB (0.0038 g, 0.01 mmol), nitric acid (6 M, 2d), DMF (4 mL) and H_2O (4 mL). The above mixture was reacted for 48 h at 90 °C. The designed product was obtained as colorless block crystal with an isolated yield of 81% that calculated based on $\text{Zn}(\text{NO}_3)_2 \cdot 6\text{H}_2\text{O}$.

Anal. Calcd. for $\text{C}_{18}\text{H}_{20}\text{N}_3\text{O}_9\text{Zn}$ (%): C, 44.32; H, 4.13; N, 8.62. Found (%): C, 44.56; H, 4.01; N, 8.83. IR (KBr, cm^{-1}): 3401 (s), 1639 (w), 1619 (vs), 1584 (m), 1534 (m), 1401 (vs), 1384 (vs), 1251 (w), 1225 (w), 1091 (w), 1065 (w), 1030 (w), 999 (w), 869 (w), 832 (m), 795 (w), 756 (w), 713 (w), 670 (w), 565 (w) (Fig. S1).

2.3. Preparation of stock solutions

The stock solutions of nitrogen containing aromatic compounds (1 mM) including 4-nitrophenylhydrazine (4-NPH), *o*-nitroaniline (*o*-NA), *m*-nitroaniline (*m*-NA), *p*-nitrophenol (*p*-NP), *o*-nitrophenol (*o*-NP), picric acid (PA) and 2,4-dinitrophenylhydrazine (2,4-DNPH) were prepared by using ethanol as the solvent. Metal ions stock solutions (Na^+ , K^+ , Zn^{2+} , Cd^{2+} , Co^{2+} , Ni^{2+} , Al^{3+} , Mg^{2+} , Pb^{2+} , Mn^{2+} , Ag^+ , Sr^{2+} , Hg^{2+} and Cu^{2+}) were prepared with the corresponding nitrate salts in deionized water with a concentration of 1 mM. The stock solutions of KMnO_4 , $\text{K}_2\text{Cr}_2\text{O}_7$ and paraquat were prepared in deionized water with a concentration of 1 mM.

2.4. Structure determination

The single-crystal data of 1 was collected on Bruker D8 Venture system, with Mo $K\alpha$ radiation ($\lambda = 0.71073 \text{ \AA}$) at 173K. All empirical absorption corrections were applied using the SCALE3 ABSPACK program [46]. The structure was solved by direct methods and refined by full-matrix least-squares analysis on F2 using the SHELX97 program

Table 1

Crystal data and structure refinements for complex 1.

Compound reference	1
Formula	$\text{C}_{18}\text{H}_{20}\text{N}_3\text{O}_9\text{Zn}$
Fw.	487.74
Crystal system	Monoclinic
Space group	$P2_1/n$
<i>a</i> (Å)	7.8233 (4)
<i>b</i> (Å)	12.5096 (4)
<i>c</i> (Å)	20.5409 (6)
α (°)	90
β (°)	92.058 (3)
γ (°)	90
<i>V</i> (Å ³)	2008.97 (13)
<i>Z</i>	4
<i>D_c</i> (g cm^{-3})	1.613
Reflections/Unique	8491/3664
<i>R</i> (int)	0.0288
GOF on F^2	1.043
^a <i>R</i> ₁ [$I \geq 2\sigma(I)$]	0.0475
^b <i>wR</i> ₂ [$I \geq 2\sigma(I)$]	0.1283

$$^a R_1 = \frac{\sum ||F_o| - |F_c||}{\sum |F_o|}$$

$$^b wR_2 = \left[\frac{\sum [w(F_o^2 - F_c^2)^2]}{\sum w(F_o^2)^2} \right]^{1/2}$$

$$\text{Where } w = 1/[2(F_o)^2 + (aP)^2 + bP] \text{ and } P = (F_o^2 + 2F_c^2)/3.$$

package. All Zn(II) atoms were first located. Then carbon, oxygen, nitrogen and hydrogen atoms of the organic framework were subsequently found. All of the non-hydrogen atoms were located from the initial solution and refined anisotropically. All calculations were performed using the SHELXTL system of computer programs [47]. Crystallographic data and structure refinements for complex 1 were displayed in Table 1. The selected bond lengths and bond angles were summarized in Table S1. CCDC reference number of complex 1 is 2027078.

3. Results and discussion

3.1. Structural characterization of complex 1

3.1.1. Structural description

Single-crystal X-ray diffraction analysis revealed that complex 1 crystallizes in monoclinic space group $P2_1/n$. The fundamental building unit of complex 1 contains one Zn(II) ion, half of cca^{2-} ligand, half of TPB ligand, one NO_3^- ion, two coordinated and two uncoordinated water molecules. In complex 1, the central Zn1(II) ion was coordinated with two chelate carboxylate oxygen atoms (O1, O2) from the cca^{2-} ligand ($\text{Zn1-O1} = 2.353(19) \text{ \AA}$ and $\text{Zn1-O2} = 2.079(9) \text{ \AA}$), two oxygen atoms (O1w, O2w) from two distinct coordinated water molecules ($\text{Zn1-O1w} = 2.199(3) \text{ \AA}$ and $\text{Zn1-O2w} = 2.153(4) \text{ \AA}$) and two nitrogen atoms (N1, N2#1) from two different TPB ligands ($\text{Zn1-N1} = 2.077(3) \text{ \AA}$ and $\text{Zn1-N2\#1} = 2.042(3) \text{ \AA}$) to form a slightly distorted octahedral coordination geometry (Fig. 1a). The styrene segment of the H_2cca ligand is disordered with the phenyl and ethenyl groups related by the crystallographic inversion symmetry (Fig. 1b). In the framework, each TPB ligand links four Zn(II) atoms to form a $[\text{Zn}(\text{TPB})_n]$ two-dimensional (2D) layer structure (Fig. 1c), which is further linked by the cca^{2-} ligands to give a 3D cationic framework with 1D channels along the *b* axis (Fig. 1d). Counterions (nitrate ions), coordinated and lattice water molecules are filled in the channels.

3.1.2. PXRD analysis

X-ray power diffraction (PXRD) patterns of complex 1 were recorded at room temperature and the results were displayed in Fig. 2. The peak positions of the as synthesized complex 1 match well with the simulated patterns, suggesting the good phase purity of complex 1.

3.1.3. TG analysis

To study the thermal stabilities of complex 1 in the temperature ranged from 20 °C to 790 °C, thermogravimetric analyses (TGA) was

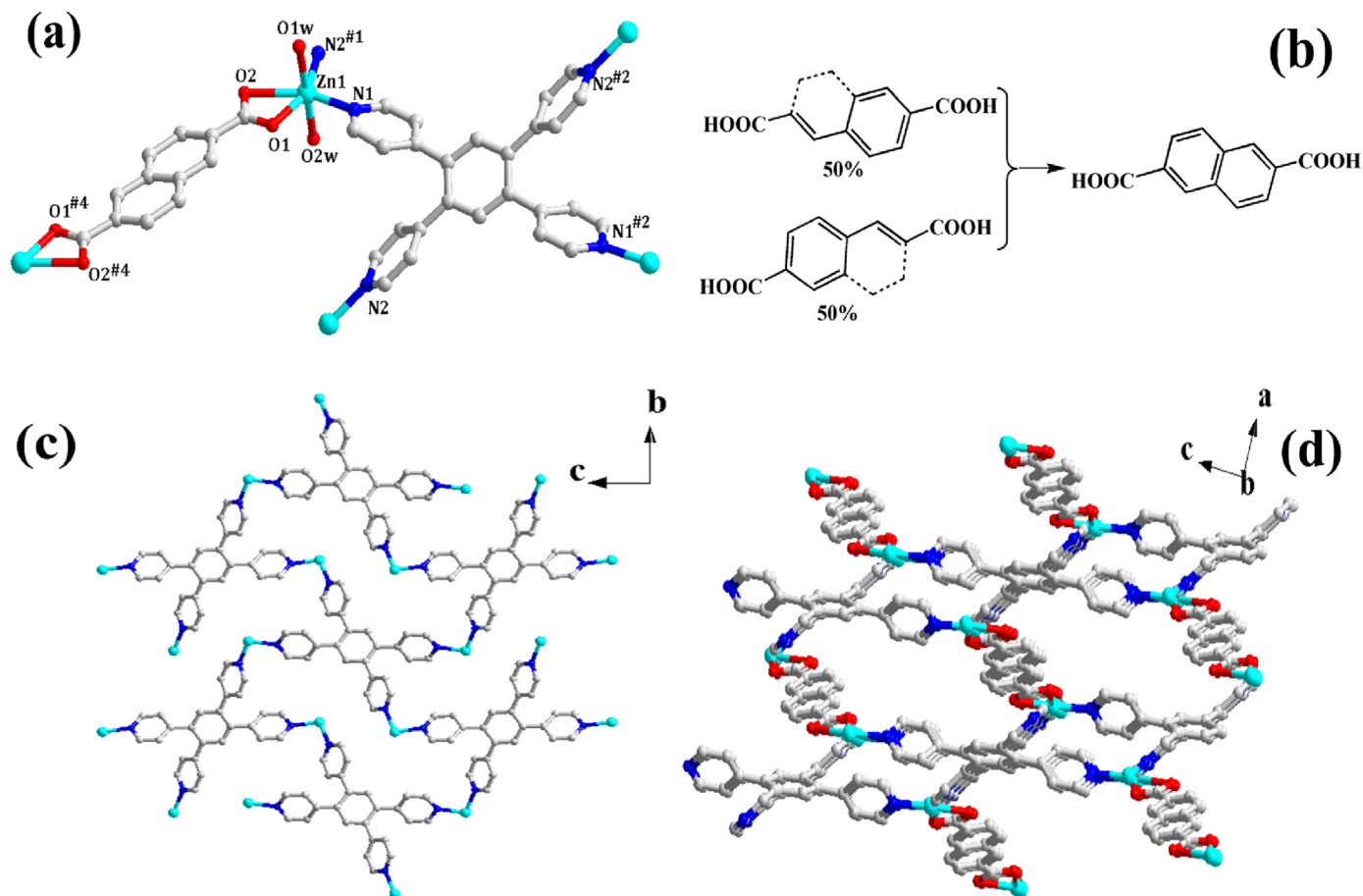


Fig. 1. (a) Coordination environments of Zn1 in complex 1, guests and hydrogen atoms are omitted for clarity. Symmetry codes: #1 - $x, -y, 1-z$; #2 - $x, 1-y, 2-z$; #3 $1/2-x, -1/2+y, 3/2-z$; #4 $1/2-x, 1/2+y, 3/2-z$; (b) View of the disorder mode of H₂cca ligand in complex 1; (c) View of the layer structure of [Zn(TPB)]_n in complex 1; (d) View of the 3D framework of complex 1 along the *ac* plane.

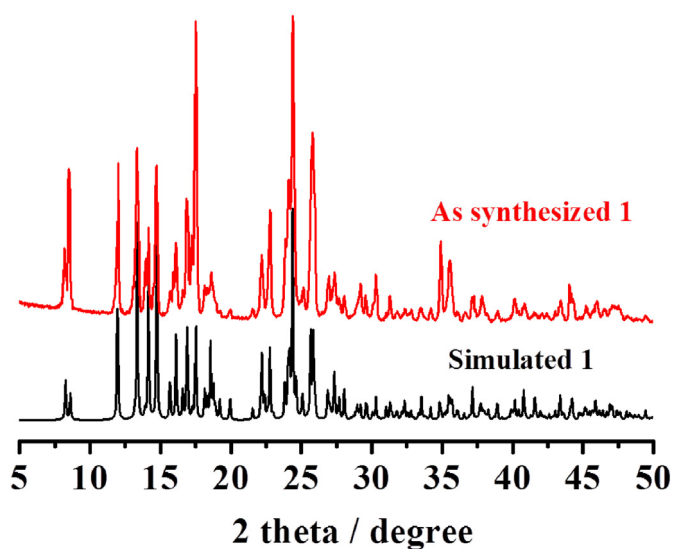


Fig. 2. PXRD patterns of complex 1.

carried out under N₂ atmosphere at a ramp rate of 10 °C min⁻¹. The result was displayed in Fig. S2, the first weight loss of 7.38% was observed from 20 °C to 100 °C in the TGA curve, which could be attributed to the release of non-coordinated water molecules (calcd 7.20%) in the channels. The

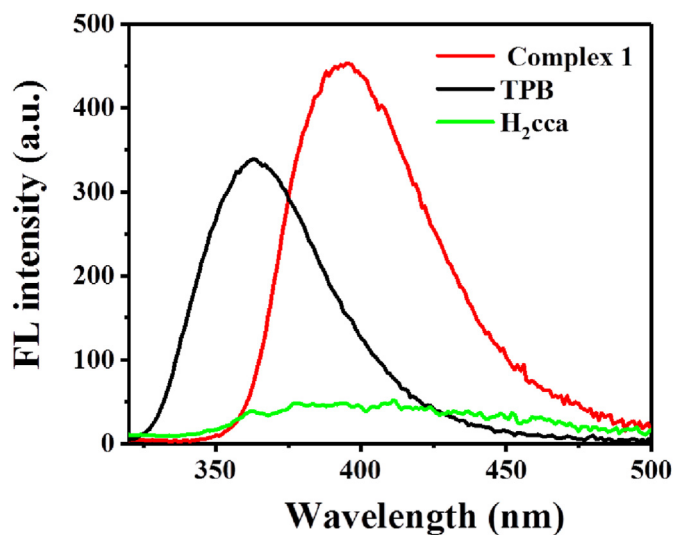


Fig. 3. Solid state fluorescent spectra of complex 1, TPB and H₂cca ($\lambda_{\text{ex}} = 300$ nm).

second weight loss is 14.77% at 100 °C–268 °C, indicating the removal of the coordinated water molecules (calcd 14.76%). Based on the TGA curve, the desolvated framework starts to collapse above 310 °C.

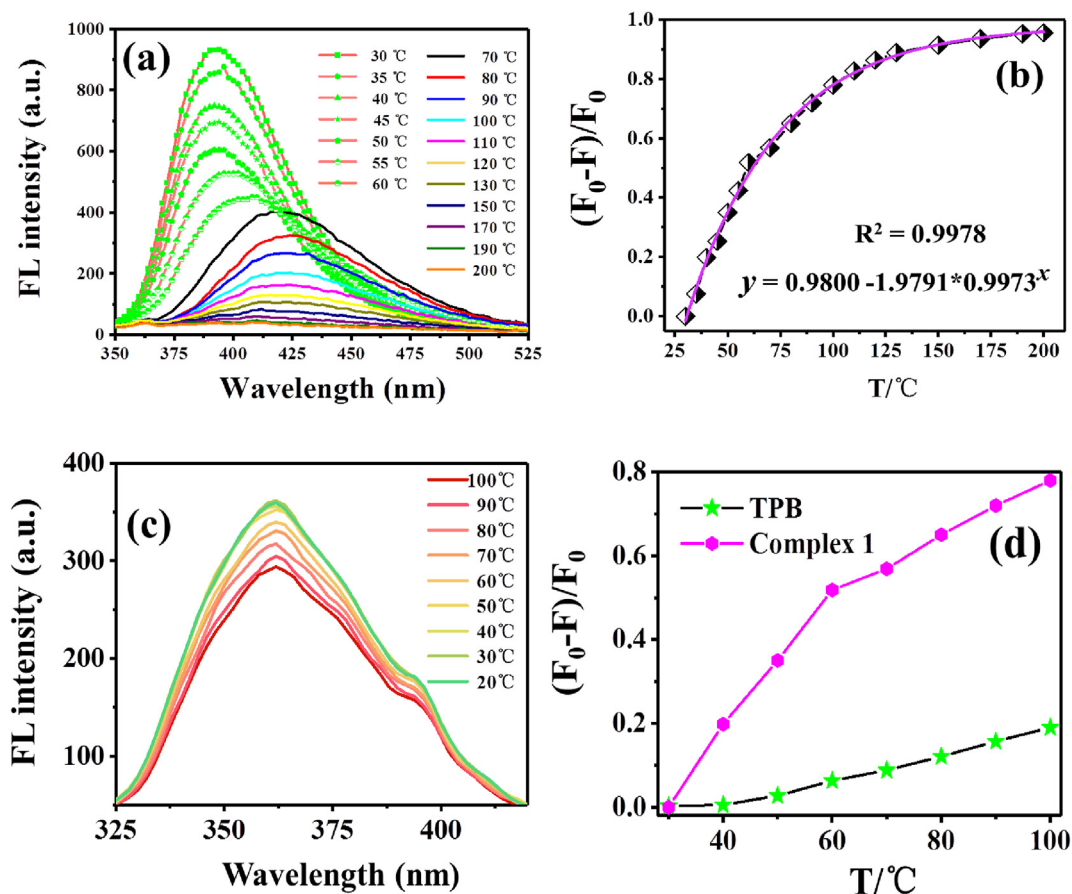


Fig. 4. (a) Solid state fluorescent spectra of complex 1 recorded on an Agilent Cary Eclipse fluorescence spectrophotometer with gradually increase temperature from 30°C to 200°C ($\lambda_{\text{ex}} = 300$ nm, slits: 2.5 nm/5 nm); (b) Solid state fluorescent quench efficiency of complex 1 at the maximum emission with temperature changed from 30°C to 200°C ($\lambda_{\text{ex}} = 300$ nm, slits: 2.5 nm/5 nm); (c) Fluorescent spectra of TPB recorded with gradually change temperature from 100°C to 20°C; (d) Fluorescent quenching efficiency of TPB and complex 1 in the temperature range from 20°C to 100°C.

3.2. Solid state fluorescent spectrum of complex 1

Initially, the solid state fluorescent of complex 1, TPB and H_2cca were recorded at room temperature. As shown in Fig. 3, H_2cca exhibited a broad weak emission upon excitation at 300 nm, while complex 1 and TPB displayed relative strong emissions with a similar shape. More specifically, a characteristic emission band centered at 400 nm was observed for complex 1 upon excited at 300 nm (Fig. 3, the red line), whereas a similar emission centered at 360 nm was observed for TPB with the same excitation (Fig. 3, the black line). Thus, complex 1 could be a linker-based luminescence MOF [1]. The emission red shift of complex 1 compared with that of TPB could be attributed to the effect of ligand-metal coordination interactions [48].

3.3. Thermo-sensitive property of complex 1

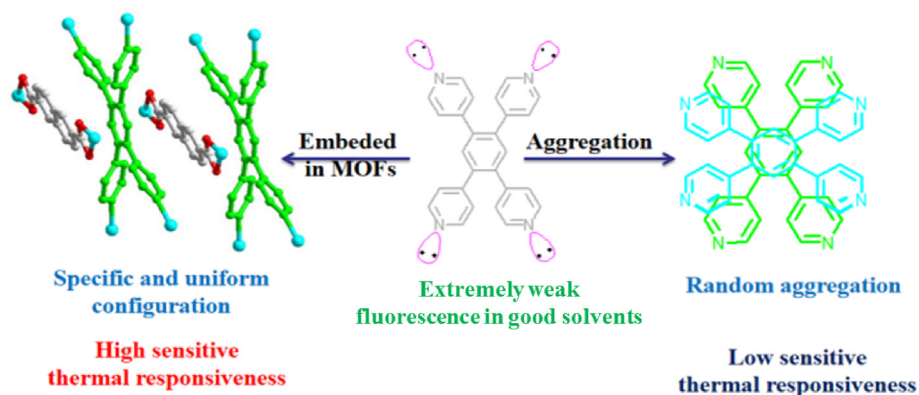
As displayed in the structural description section, each TPB ligand links four Zn(II) atoms to form a $[\text{Zn}(\text{TPB})]_n$ two-dimensional (2D) layer structure (Fig. 1c), which is further linked by the cca^{2-} ligands to give rise to the 3D cationic framework (Fig. 1d). Due to the flexible nature of H_2cca ligands, complex 1 exhibits a relative flexible framework which lead to the disorder of cca^{2-} in complex 1 (Fig. 1b). Meanwhile, due to the lone pair electrons in TPB served as the coordination sites, the rotation of pyridine rings will not destroy the framework of complex 1. In addition, according to the literature, flexible frameworks are more sensitive to the physical or chemical stimuli [26,27]. Thus, in order to reveal the potential temperature responsive property, the solid state fluorescent spectra of complex 1 were recorded with gradually increase the ambient temperature.

As shown in Fig. 4a, complex 1 exhibited remarkable fluorescent response to the variation of temperature. The fluorescent emission centered at 395 nm gradually quenched with the ambient temperature changed from 30°C to 200°C. Interestingly, a noticeable peak shift from 395 nm to 420 nm was recorded in the fluorescent emission spectra with the environmental temperature changed from 30°C to 70°C [49,50]. According to the TG analysis, the non-coordinated water molecules in the channels of complex 1 were released before 100°C, which might lead to the structure transformation and finally result in the emission red shift. Further increasing the ambient temperature from 80°C to 200°C only resulted in fluorescent quenching and no obvious shift was observed. In addition, the fluorescent emission almost completely quenched when the ambient temperature reached to 200°C, revealing the decay was dominated by non-radiative processes at that temperature [51,52].

The maximum emission intensities of complex 1 were shown in Fig. S3. The corresponding fluorescent quenching efficiency was obtained by using the following equation: $(F_0 - F)/F_0$ [53] and the results were illustrated in Fig. 4b. Non-linear fitting analysis for the fluorescent quenching efficiency versus the temperature was performed. As shown in Fig. 4b, the fluorescent quenching efficiency fitted well with the non-linear equation: $y = 0.9800 - 1.9791 \times 0.9973^x$ ($R^2 = 0.9978$, where x represents the ambient temperature and y represents $(F_0 - F)/F_0$), which suggested that complex 1 might be used as a fluorescent thermometer (Fig. S10).

3.3.1. Plausible mechanism for the sensitive thermal responsiveness

For comparison, the fluorescent emission spectra of TPB changed from 100°C to 20°C were recorded. As displayed in Fig. 4c, the fluorescent intensity of TPB slowly enhanced with the ambient temperature



Scheme 1. A possible mechanism for the enhanced thermal sensitivity of complex 1.

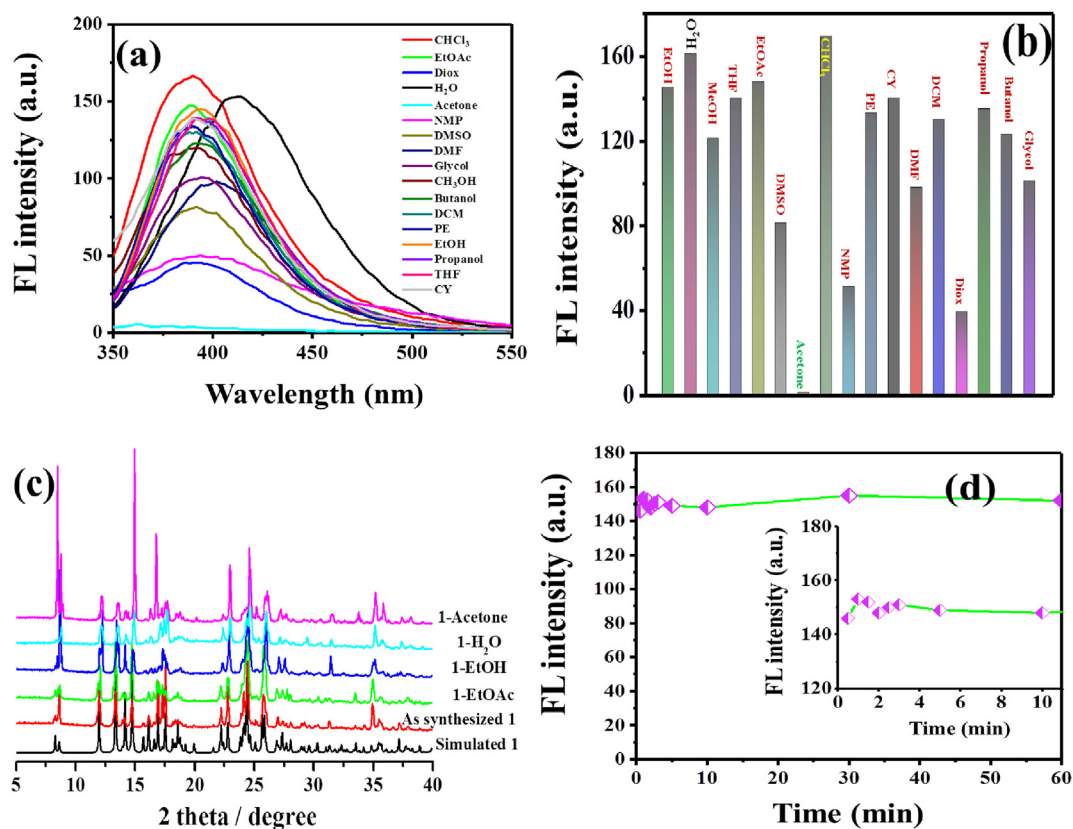


Fig. 5. (a) Fluorescent spectra of complex 1 after dispersed in various solvents; (b) The maximum fluorescent intensity of complex 1 after dispersed in different solvents ($\lambda_{em} = 420$ nm in water, $\lambda_{em} = 400$ nm in DMF, $\lambda_{em} = 390$ nm in other solvents, slits: 5 nm/5 nm); (c) PXRD patterns of the recycled complex 1; (d) Fluorescent intensities of complex 1-H₂O suspension ($\lambda_{em} = 420$ nm) at different time after dispersed in water (insert, the enlarged view of fluorescent intensity changes in 10 min).

decreased. The fluorescent quenching efficiency of TPB and complex 1 in the temperature range from 20°C to 100°C were shown in Fig. 4d. Apparently, the fluorescent quenching efficiency of complex 1 sharply increased to 79% when the ambient temperature reached 100°C, while the fluorescent quenching efficiency of free TPB ligands is below 20% at that temperature. Thus, the thermo-sensitivity of TPB could be enhanced by embedding into the framework of MOF. A possible mechanism to rationalize these results is proposed in Scheme 1.

In the framework of complex 1, the TPB ligands displayed a specific and uniform configuration (Scheme 1 and Fig. 1d) which will enhance the sensitivity of thermal responsiveness, just as the proverb goes “united we stand, divided we fall”. However, the free TPB ligands displayed a

random aggregation which would lead to low sensitive thermal responsiveness (Scheme 1).

3.4. Fluorescent sensing property of complex 1 in solvents

3.4.1. Solvents screening

In order to find suitable dispersion mediums for further sensing applications, the fluorescent spectra of complex 1 were recorded after dispersed in different solvents. As shown in Fig. 5a, complex 1 suspensions exhibited characteristic emission of complex 1 in solvents including ethanol (EtOH), water (H₂O), methanol (MeOH), tetrahydrofuran (THF), ethyl acetate (EtOAc), dimethyl sulfoxide (DMSO), acetone, chloroform

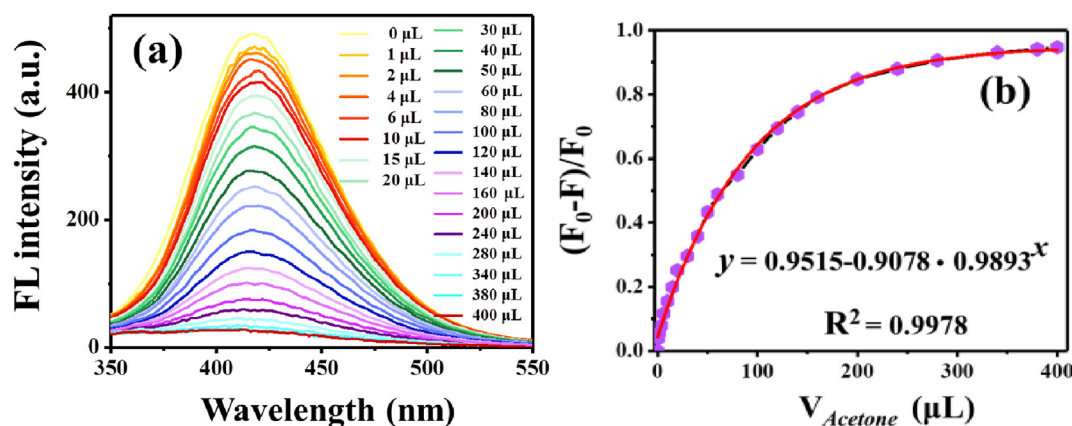


Fig. 6. (a) Fluorescent spectra of complex 1-H₂O suspension (3 mL) with different concentration of acetone ($\lambda_{\text{ex}} = 300$ nm, slits: 5 nm/10 nm); (b) Fluorescent quenching efficiency of complex 1-H₂O suspension with different concentration of acetone ($\lambda_{\text{ex}} = 300$ nm, $\lambda_{\text{em}} = 420$ nm, slits: 5 nm/10 nm).

(CHCl₃), N-methyl-2-pyrrolidone (NMP), petroleum ether (PE), cyclohexane (CY), N,N-dimethylformamide (DMF), dichloromethane (DCM), dioxane (Diox), propanol, butanol, glycol. Although the fluorescent intensity changed to some extent, no obvious emission shift was observed for the above suspensions. However, a remarkable red shift from 390 nm to 420 nm was observed when water (H₂O) was used as the dispersion medium (Fig. 5a, the black line). In addition, the fluorescent almost completely quenched when acetone was used as the dispersion medium.

The maximum fluorescent intensity of the above suspensions were recorded and displayed in Fig. 5b. Interestingly, strong fluorescent emissions were observed both in water and organic solvents, which suggested that complex 1 could be used in both hydrophilic and hydrophobic environments. In order to reveal the stability of complex 1 in solvents, PXRD tests for those samples that recycled from acetone, ethanol, EtOAc and water were performed. As shown in Fig. 5c, PXRD patterns of the recycled complex 1 match well with the simulated one based on the single-crystal diffraction data, which confirming the good stability of complex 1 in solvents (Fig. 5c).

The stability of complex 1-H₂O suspension was further revealed by recording the fluorescent spectra of complex 1 at different time after dispersed in water. As displayed in Fig. 5d, the fluorescent intensity of complex 1-H₂O suspension ($\lambda_{\text{em}} = 420$ nm) reached a stable level in less than 2 min (Fig. 5d, insert), and no obvious change was observed after dispersed for 1 h (Fig. 5d). In addition, the good fluorescent stability of complex 1 in water was consistent with the structural stability that revealed by the PXRD tests (Fig. 5c, the 1-H₂O line).

3.4.2. Fluorescent detection of acetone in water

According to the solvent screening (Fig. 5a, d) and PXRD test (Fig. 5c) results, complex 1 displayed remarkable fluorescent quenching in acetone and good fluorescent stability in water. In order to reveal the potential application of complex 1 in the fluorescent sensing of contaminants in water, fluorescent titration experiments were performed.

Fluorescent spectra of complex 1-H₂O suspension (3 mL) were recorded with gradually addition of acetone. As shown in Fig. 6a, the fluorescent emission of complex 1-H₂O suspension gradually quenched with the increasing of acetone concentration. Much to our surprise, a noticeable fluorescent quenching has been observed for complex 1-H₂O suspension after treatment with 1 μL acetone (0.03 vol%), which revealing the high sensitivity of complex 1 in the fluorescent sensing of acetone. In addition, the fluorescent intensity of complex 1-H₂O suspension centered at 420 nm was recorded with gradually addition of acetone (Fig. S4).

Correspondingly, the fluorescent quenching efficiency of complex 1-H₂O suspension was calculated by using the equation: $(F_0 - F)/F_0$. As can be seen from Fig. 6b, the fluorescent quenching presented a “fast followed by slow” trend. It is worth mentioning that the quenching efficiency have

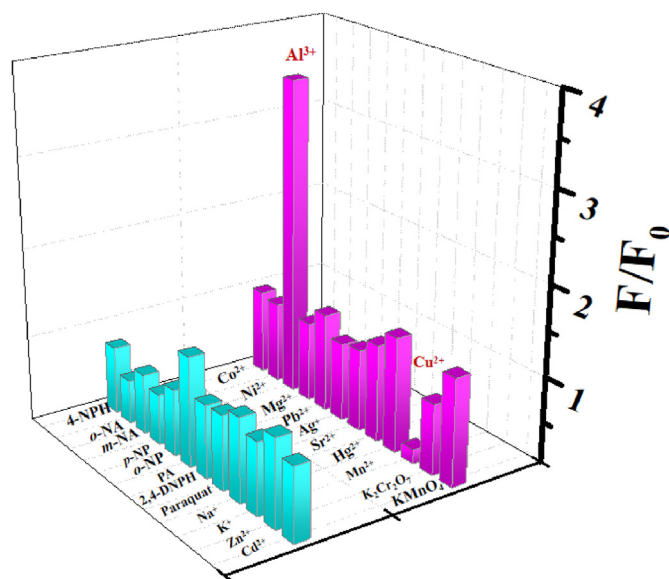


Fig. 7. Fluorescent intensities change of complex 1-H₂O suspensions after treatment with 50 μM various analytes (F/F_0 , where F is the fluorescent intensity of complex 1-H₂O suspension after treatment with analyt and F_0 is the fluorescent intensity of complex 1-H₂O suspension in the absence of analyt, $\lambda_{\text{ex}} = 300$ nm, $\lambda_{\text{em}} = 420$ nm, slits: 5 nm/5 nm).

reached 63% with 100 μL acetone (3.2 vol%) and 95% with 100 μL acetone (11.7 vol%), respectively. Quantitative relation analysis was performed and displayed in Fig. 6b. Interestingly, the fluorescent quenching efficiency of complex 1-H₂O suspension versus the concentration of acetone fitted well with the follow non-linear equation: $y = 0.9515 - 0.9078 \times 0.9893^x$ ($R^2 = 0.9978$, where x represents the concentration of acetone and y represents the fluorescent quenching efficiency), which revealed that complex 1-H₂O suspension could be used in the quantitatively sensing acetone in water. In addition, the real-time fluorescent quenching sensing of acetone in water could be explained with the inner filter effect (IFE) between complex 1 and acetone. As displayed in Fig. S5, the absorbance spectrum of acetone well overlapped with that of complex 1. The excitation light would be competitively absorbed by acetone and result in the sharp fluorescent quenching of complex 1.

3.4.3. Fluorescent detection of metal ions in water

3.4.3.1. Selectivity study. With the above results in hand, the stable complex 1-H₂O suspensions were treated with various analytes (50 μM)

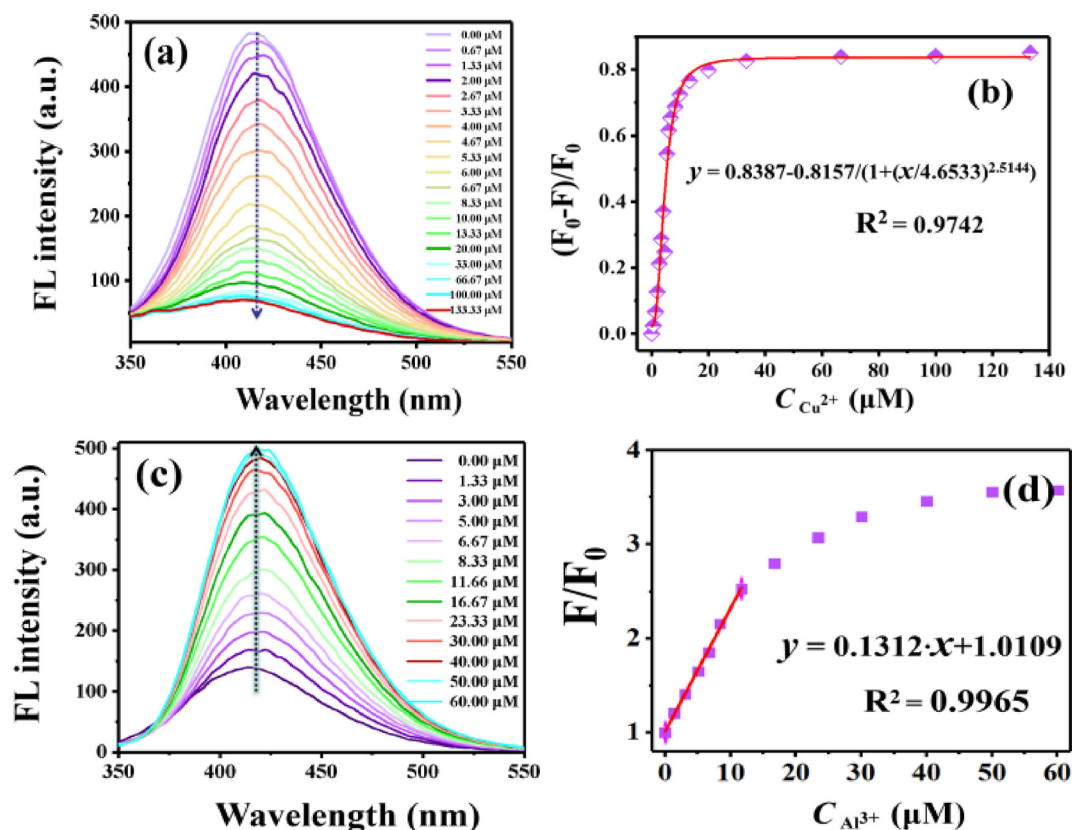


Fig. 8. (a) Fluorescent spectra of complex 1-H₂O suspension after treatment with different concentration of Cu²⁺; (b) Fluorescent quenching efficiency of complex 1-H₂O suspension after treatment with different concentration of Cu²⁺ ($\lambda_{\text{ex}} = 300$ nm, slits: 5 nm/10 nm); (c) Fluorescent spectra of complex 1-H₂O suspension after treatment with different concentration of Al³⁺; (d) Fluorescent intensity changes of complex 1-H₂O suspension (F/F₀) after treatment with different concentration of Al³⁺ ($\lambda_{\text{ex}} = 300$ nm, $\lambda_{\text{em}} = 420$ nm, slits: 5 nm/5 nm).

including metal ions, explosives, paraquat, KMnO₄ and K₂Cr₂O₇ to investigate their fluorescent responses. Fluorescent intensity change of complex 1-H₂O suspensions centered at 420 nm (F/F₀, where F₀ represents the initial fluorescent intensity of complex 1-H₂O suspension, F represents the fluorescent intensity of complex 1-H₂O suspension after treatment with analyte) was recorded and displayed in Fig. 7 and Fig. S11. As can be seen from Fig. 7, although the value of F/F₀ changed to some extent with the variation of analytes, no remarkable response was observed for most of the analytes including explosives, Na⁺, K⁺, Zn²⁺, Cd²⁺, Co²⁺, Ni²⁺, Mg²⁺, Mn²⁺, Pb²⁺, Ag⁺, Sr²⁺, Hg²⁺, KMnO₄, K₂Cr₂O₇ and paraquat (F/F₀ was approximately equal to 1.0). However, noticeable fluorescent enhancements were observed for complex 1-H₂O suspensions after treatment with Al³⁺ (F/F₀ = 3.60), while remarkable fluorescent quenching effect was observed after treatment with Cu²⁺ (F/F₀ = 0.12). In addition, good selectivity was also observed in the interference experiment (Fig. S11).

3.4.3.2. Sensitivity study. In order to reveal the sensitivity of complex 1 in the fluorescent detection Cu²⁺ and Al³⁺ in water, fluorescent titration experiments were carried out. Initially, fluorescent spectra of complex 1-H₂O suspensions were recorded with gradually addition of Cu²⁺. As displayed in Fig. 8a, the fluorescent emission of complex 1-H₂O suspension was gradually quenched with the increasing of Cu²⁺ concentration. Delightfully, remarkable fluorescent quenching has already been observed for complex 1-H₂O suspension after treatment with 0.67 μM Cu²⁺, revealing the good sensitivity of complex 1 in the fluorescent sensing of Cu²⁺. Fluorescent intensities of the above complex 1-H₂O suspension were recorded and displayed in Fig. S6. The corresponding fluorescent quenching efficiency was calculated by using the following equation: (F₀-F)/F₀. As shown in Fig. 8b, quick fluorescent quenching

was observed in the concentration range from 0.67 μM to 20 μM. And no obvious quenching was observed with further increasing Cu²⁺ concentration to 100 μM. In addition, the fluorescent quenching efficiency versus the concentration of Cu²⁺ fit well with the nonlinear equation: $y = 0.8387 - 0.8157 / (1 + (x/4.6533)^{2.5144})$ ($R^2 = 0.9742$, where y represents the fluorescent quenching efficiency and x represents the concentration of Cu²⁺).

Sensitivity of complex 1 in the fluorescence-enhanced detection of Al³⁺ was revealed by the fluorescence titration experiments. As illustrated in Fig. 8c, with the increasing of ions concentration, significant fluorescence enhancements were observed. Interestingly, noticeable fluorescent intensity change has already been recorded for complex 1-H₂O suspensions after treatment with 1.33 μM Al³⁺. The above noticeable fluorescent responses revealed the high sensitivity of this method. Fluorescent intensities of complex 1-H₂O suspensions ($\lambda_{\text{em}} = 420$ nm) after treatment with different concentration of Al³⁺ were illustrated in Fig. S8.

Correspondingly, the fluorescent intensity changes (F/F₀) of complex 1-H₂O suspensions were calculated. As can be seen from Fig. 8d, good linear relationship was observed between the fluorescent changes (F/F₀) and the ion concentration. More specifically, the linear concentration range of Al³⁺ ranged from 0 μM to 11.7 μM with a correlation equation of $y = 0.1312 \cdot x + 1.0109$ ($R^2 = 0.9965$, where y represents the fluorescent intensity change F/F₀ and x represents the concentration of Al³⁺).

3.5. Plausible sensing mechanisms

According to previous reports, the paramagnetic Cu²⁺ could engage in the electron transfer process of ligands in MOFs due to its open-shell d-orbitals (3d⁹) [54]. After treatment with Cu²⁺, the electron transfer

between TPB ligands (TPB) would be inhibited and energy transfer between complex 1 and Cu^{2+} might occur, which will lead to fluorescence quenching. In order to confirm the energy transfer between complex 1 and Cu^{2+} , luminescence lifetime test for complex 1 in the absence and presence Cu^{2+} were performed. As shown in Fig. S7, the lifetime of complex 1 is about 2.46 ns. However, when Cu^{2+} is added into complex 1 suspension, the lifetime of complex 1 reduced to about 1.31 ns. The above results confirmed that energy transfer occurred between complex 1 and Cu^{2+} , which would lead to fluorescence quenching [54]. In addition, it has been pointed out in previous literature that Al^{3+} could make energy transfer process more effective and lead to the fluorescent enhancement [55]. In order to verify this possibility, the fluorescent intensity of the free ligand (TPB) in ethanol were recorded in the absence and presence of Al^{3+} . As shown in Fig. S9, the fluorescent intensity of TPB obviously enhanced after treatment with Al^{3+} . Thus, fluorescent enhancements in the detection of Al^{3+} might due to more efficient energy transfer from ligand to ligand occurred promoted by Al^{3+} .

4. Conclusions

A novel 3D fluorescent Zn-MOF (complex 1) has been rationally designed and its multipurpose applications have been revealed. The structure of complex 1 was fully characterized by XRD, TG, FT-IR and PXRD analysis. Complex 1 exhibited strong fluorescent emission in both solid state and in solvents. By embedding TPB into the framework, high sensitive thermal responsiveness was observed in a wide temperature ranged from 30°C to 200°C. Good nonlinear relationship was observed between the fluorescent quenching efficiency and the ambient temperature, which suggested that complex 1 might be used as a quantitative fluorescent thermometer. Besides, stable complex 1-H₂O suspension was obtained and used in the real-time fluorescent sensing of acetone in water with an experimental detection limit of 0.03% (vol. %). Moreover, complex 1-H₂O suspension exhibited promising potential in the fluorescent enhancement sensing of Al^{3+} and fluorescent quenching sensing of Cu^{2+} in water with good selectivity and sensitivity. In addition, the proposed method might be used as a general methodology for the preparation of luminescence MOF thermometers.

CRedit authorship contribution statement

Ensheng Zhang: Data curation, Writing – review & editing, Supervision. **Long Jiang:** Conceptualization, Resources. **Ruijiang Lv:** Formal analysis. **Shiyang Li:** Investigation. **Rongmei Kong:** Methodology. **Lian Xia:** Formal analysis. **Ping Ju:** Supervision, Methodology, Investigation, Resources, Writing – original draft. **Fengli Qu:** Funding acquisition, Formal analysis.

Declaration of competing interest

The authors declare that they have no known competing financial interests or personal relationships that could have appeared to influence the work reported in this paper.

Acknowledgements

This work was financially supported by National Natural Science Foundation of China (22007055, 21775089, 22074080), Natural Science Foundation of Shandong Province of China (ZR2020QB156), Changjiang Scholar Program of the Ministry of Education of China (Q2019258), Taishan Scholar Program of Shandong Province (tsqn201909106), and the Startup Foundation for Doctors of Qufu Normal University.

Appendix A. Supplementary data

Supplementary data to this article can be found online at <https://doi.org/10.1016/j.jssc.2021.122476>.

References

- [1] Y.M. Zhang, S. Yuan, G. Day, X. Wang, X.Y. Yang, H.C. Zhou, Luminescent sensors based on metal-organic frameworks, *Coord. Chem. Rev.* 354 (2018) 28–45.
- [2] N. Stock, S. Biswas, Synthesis of metal-organic frameworks (MOFs): routes to various MOF topologies, morphologies, and composites, *Chem. Rev.* 112 (2012) 933–969.
- [3] S. Sharma, S. Let, A.V. Desai, S. Dutta, G. Karuppusamy, M.M. Shirolkar, R. Barabao, S.K. Ghosh, Rapid, selective capture of toxic oxo-anions of Se(IV), Se(VI) and As(V) from water by an ionic metal organic framework (iMOF), *J. Mater. Chem. A* 9 (2021) 6499–6507.
- [4] W.P. Lustig, S. Mukherjee, N.D. Rudd, A.V. Desai, J. Li, S.K. Ghosh, Metal-organic frameworks: functional luminescent and photonic materials for sensing applications, *Chem. Soc. Rev.* 46 (2017) 3242–3285.
- [5] F.Y. Zhong, X. Zhang, C.Q. Zheng, H. Xu, J.K. Gao, S.Q. Xu, A fluorescent titanium-based metal-organic framework sensor for nitroaromatics and nanomolar Fe^{3+} detection, *J. Solid State Chem.* (2020) 121391.
- [6] S.S. Zhao, J. Yang, Y.Y. Liu, J.F. Ma, Fluorescent aromatic Tag-functionalized MOFs for highly selective sensing of metal ions and small organic molecules, *Inorg. Chem.* 55 (2016) 2261–2273.
- [7] J.P. Lei, R.C. Qian, P.H. Ling, L. Cui, H.X. Ju, Design and sensing applications of metal-organic framework composites, *Trac. Trends Anal. Chem.* 58 (2014) 71–78.
- [8] L.L. Zhang, Z.X. Kang, X.L. Xin, D.F. Sun, Metal-organic frameworks based luminescent materials for nitroaromatics sensing, *CrystEngComm* 18 (2016) 193–206.
- [9] H. Wang, W.T. Yang, Z.M. Sun, Mixed-ligand Zn-MOFs for highly luminescent sensing of nitro compounds, *Chem. Asian J.* 8 (2013) 982–989.
- [10] B. Gole, A.K. Bar, P.S. Mukherjee, Fluorescent metal-organic framework for selective sensing of nitroaromatic explosives, *Chem. Commun.* 47 (2011) 12137–12139.
- [11] N.A. Khan, Z. Hasan, S.H. Jung, Adsorptive removal of hazardous materials using metal-organic frameworks (MOFs): a review, *J. Hazard Mater.* 244 (2013) 444–456.
- [12] C.T. Yang, G. Miao, Y.H. Pi, Q.B. Xia, J.L. Wu, Z. Li, J. Xiao, Abatement of various types of VOCs by adsorption/catalytic oxidation: a review, *Chem. Eng. J.* 370 (2019) 1128–1153.
- [13] S. Homayoonnia, S. Zeinali, Design and fabrication of capacitive nanosensor based on MOF nanoparticles as sensing layer for VOCs detection, *Sensor. Actuator. B Chem.* 237 (2016) 776–786.
- [14] Y. Li, A.S. Xiao, B. Zou, H.X. Zhang, K.L. Yan, Y. Lin, Advances of metal-organic frameworks for gas sensing, *Polyhedron* 154 (2018) 83–97.
- [15] K. Pawan, A. Deep, K.H. Kim, Metal organic frameworks for sensing applications, *Trac. Trends Anal. Chem.* 73 (2015) 39–53.
- [16] X. Zhu, H.Y. Zheng, X.F. Wei, Z.Y. Lin, L.H. Guo, B. Qiu, G.N. Chen, Metal-organic framework (MOF): a novel sensing platform for biomolecules, *Chem. Commun.* 49 (2013) 1276–1278.
- [17] Z.H. Jiao, X.L. Jiang, S.L. Hou, M.H. Tang, B. Zhao, Highly sensitive and selective luminescence sensor based on two fold interpenetrated MOFs for detecting glutamate in serum, *Inorg. Chem.* 59 (2020) 2171–2177.
- [18] A. Clearfield, Flexible MOFs under stress: pressure and temperature, *Dalton Trans.* 45 (2016) 4100–4112.
- [19] A.L. Robinson, V. Stavila, T.R. Zeitler, M.I. White, S.M. Thornberg, J.A. Greathouse, M.D. Allendorf, Ultrasensitive humidity detection using metal-organic framework-coated microsensors, *Anal. Chem.* 84 (2012) 7043–7051.
- [20] J. Liu, F. Sun, F. Zhang, Z. Wang, R. Zhang, C. Wang, S. Qiu, In situ growth of continuous thin metal-organic framework film for capacitive humidity sensing, *J. Mater. Chem.* 21 (2011) 3775–3778.
- [21] K.W. Chapman, G.J. Halder, P.J. Chupas, Pressure-induced amorphization and porosity modification in a metal-organic framework, *J. Am. Chem. Soc.* 131 (2009) 17546–17547.
- [22] K.B. Wang, R. Bi, M.L. Huang, B. Lv, H.J. Wang, C. Li, H. Wu, Q.C. Zhang, Porous cobalt metal-organic frameworks as active elements in battery-supercapacitor hybrid devices, *Inorg. Chem.* 59 (2020) 6808–6814.
- [23] K.B. Wang, Q.Q. Li, Z.J. Ren, C. Li, Y. Chu, Z.K. Wang, M.D. Zhang, H. Wu, Q.C. Zhang, 2D metal-organic frameworks (MOFs) for high-performance BatCap hybrid devices, *Small* 16 (2020) 2001987.
- [24] K.B. Wang, S.E. Wang, J.D. Liu, Y.X. Guo, F.F. Mao, H. Wu, Q.C. Zhang, Fe-based coordination polymers as battery-type electrodes in semi-solid-state battery-supercapacitor hybrid devices, *ACS Appl. Mater. Interfaces* 13 (2021) 15315–15323.
- [25] K.B. Wang, Z.K. Wang, J.D. Liu, C. Li, F.F. Mao, H. Wu, Q.C. Zhang, Enhancing the performance of a battery-supercapacitor hybrid energy device through narrowing the capacitance difference between two electrodes via the utilization of 2D MOF-nanosheet-derived Ni@nitrogen-doped-carbon core-shell rings as both negative and positive electrodes, *ACS Appl. Mater. Interfaces* 12 (2020) 47482–47489.
- [26] A. Schneemann, V. Bon, I. Schwedler, I. Senkovska, S. Kaskel, R.A. Fischer, Flexible metal-organic frameworks, *Chem. Soc. Rev.* 43 (2014) 6062–6096.
- [27] Z. Chang, D.H. Yang, J. Xu, T.L. Hu, X.H. Bu, Flexible metal-organic frameworks: recent advances and potential applications, *Adv. Mater.* 27 (2015) 5432–5441.
- [28] J. Wieme, K. Lejaeghere, G. Kresse, V. Van Speybroeck, Tuning the balance between dispersion and entropy to design temperature-responsive flexible metal-organic frameworks, *Nat. Commun.* 9 (2018) 1–10.
- [29] M.L. Shen, L. Xu, B. Liu, H. Jiao, Y.U. Kwon, Thermosensitive fluorescent Eu-based metal-organic framework and its polyether sulfone composite film as thermal sensor, *Dalton Trans.* 47 (2018) 8330–8336.

- [30] Y. Yang, Y.Z. Wang, Y. Feng, X.R. Song, C. Cao, G.L. Zhang, W.S. Li, Three isostructural $\text{Eu}^{3+}/\text{Tb}^{3+}$ co-doped MOFs for wide-range ratiometric temperature sensing, *Talanta* 208 (2020) 120354.
- [31] Y. Hasegawa, Y. Kitagawa, Thermo-sensitive luminescence of lanthanide complexes, clusters, coordination polymers and metal-organic frameworks with organic photosensitizers, *J. Mater. Chem. C* 7 (2019) 7494–7511.
- [32] D. Zhao, D. Yue, K. Jiang, L. Zhang, C.X. Li, Isostructural $\text{Tb}^{3+}/\text{Eu}^{3+}$ co-doped metal-organic framework based on pyridine-containing dicarboxylate ligands for ratiometric luminescence temperature sensing, *Inorg. Chem.* 58 (2019) 2637–2644.
- [33] J. Rocha, C.D. Brites, L.D. Carlos, Lanthanide organic framework luminescent thermometers, *Chem. Eur. J.* 22 (2016) 14782–14795.
- [34] H. Li, W. Han, R. Lv, A. Zhai, X.L. Li, W. Gu, X. Liu, Dual-function mixed-lanthanide metal-organic framework for ratiometric water detection in bioethanol and temperature sensing, *Anal. Chem.* 91 (2019) 2148–2154.
- [35] J. Liang, B.Z. Tang, B. Liu, Specific light-up bioprobes based on AIEgen conjugates, *Chem. Soc. Rev.* 44 (2015) 2798–2811.
- [36] Q. Zeng, Z. Li, Y.Q. Dong, C.A. Di, A.J. Qin, Y.N. Hong, L. Ji, Z.C. Zhu, C.K.W. Jim, G. Yu, Q.Q. Li, Z.A. Li, Y.Q. Liu, J.G. Qin, B.Z. Tang, Fluorescence enhancements of benzene-cored luminophors by restricted intramolecular rotations: AIE and AIEE effects, *Chem. Commun.* 1 (2007) 70–72.
- [37] E.S. Zhang, X.F. Hou, Z. Zhang, Y.Q. Zhang, J.J. Wang, H. Yang, J.M. You, P. Ju, A novel biomass-based reusable AIE material: AIE properties and potential applications in amine/ammonia vapor sensing and information storage, *J. Mater. Chem. C* 7 (2019) 8404–8411.
- [38] B. Ji, W. Wang, D. Deng, Y. Zhang, L. Cao, L. Zhou, C.S. Ruan, T.S. Li, Structural competition between $\pi\cdots\pi$ interactions and halogen bonds: a crystallographic study, *CrystEngComm* 15 (2013) 769–774.
- [39] E.T. Nguyen, X. Zhao, D. Ta, P.L. Nguyen, X.H. Bu, Comparative study of in situ and presynthesized X-pillar ligand in self-assembly of homochiral porous frameworks, *Cryst. Growth Des.* 15 (2015) 5939–5944.
- [40] J.X. Meng, Y.G. Li, H. Fu, X.L. Wang, E.B. Wang, Controllable self-assembly of two novel metal-organic frameworks based on different tetradentate in situ ligands, *CrystEngComm* 13 (2011) 649–655.
- [41] S. Hu, J.C. Chen, M.L. Tong, B. Wang, Y.X. Yan, S.R. Batten, Cu^{2+} -Mediated dehydrogenative coupling and hydroxylation of an n-heterocyclic ligand: from generation of a new tetrapotic ligand to the designed assembly of three-dimensional copper (I) coordination polymers, *Angew. Chem. Int. Ed.* 44 (2005) 5471–5475.
- [42] Z.G. Han, Y.P. Liu, X.F. Zhao, J.S. Yan, X.L. Zhai, Polyanionic clusters embedded in lattice-type hydrogen bonding networks involving in situ bond activation and coupling of organic cations, *CrystEngComm* 17 (2015) 7339–7345.
- [43] N.F. Zheng, X.H. Bu, P.Y. Feng, Self-assembly of novel dye molecules and $[\text{Cd}_8(\text{SPH})_{12}]^{4+}$ cubic clusters into three-dimensional photoluminescent superlattice, *J. Am. Chem. Soc.* 124 (2002) 9688–9689.
- [44] S. Hu, Z.M. Zhang, Z.S. Meng, Z.J. Lin, M.L. Tong, Anion-dependent construction of copper(I/II)-1,2,4,5-tetra(4-pyridyl)benzene frameworks, *CrystEngComm* 12 (2010) 4378–4385.
- [45] W. Liu, C.C. Chen, L.L. Mao, S.G. Wu, L.F. Wang, M.L. Tong, Tuning the net topology of a ternary $\text{Ag(I)-1,2,4,5-tetra(4-pyridyl)}$ benzene-carboxylate framework: structures and photoluminescence, *CrystEngComm* 21 (2019) 6446–6451.
- [46] G.M. Sheldrick, SADABS, Program for Empirical Absorption Correction of Area Detector Data, University of Göttingen, Göttingen, 1996.
- [47] G.M. Sheldrick, SHELXS 97, Program for Crystal Structure Refinement, University of Göttingen, Göttingen, 1997.
- [48] Y.L. Wu, G.P. Yang, Y.Q. Zhao, W.P. Wu, B. Liu, Y.Y. Wang, Three new solvent-directed Cd(II) -based MOFs with unique luminescent properties and highly selective sensors for Cu^{2+} cations and nitrobenzene, *Dalton Trans.* 44 (2015) 3271–3277.
- [49] T.G. Sun, Z.L. Gong, J.Y. Shao, Y.W. Zhong, A star-shaped solvatofluorochromic pyrene-triarylamine derivative as a fluorescent thermometer over a wide temperature range, *Chin. J. Chem.* 38 (2020) 1515–1520.
- [50] S.X. Tang, N. Wang, X.D. Xu, S.Y. Feng, A ratiometric fluorescent thermometer based on amphiphilic alkynylpyrene derivatives, *New J. Chem.* 43 (2019) 6461–6464.
- [51] Q. Zeng, Z. Li, Y.Q. Dong, C.A. Di, A.J. Qin, Y.N. Hong, L. Ji, Z.C. Zhu, C.K.W. Jim, G. Yu, Q.Q. Li, Z.A. Li, Y.Q. Liu, J.G. Qin, B.Z. Tang, Fluorescence enhancements of benzene-cored luminophors by restricted intramolecular rotations: AIE and AIEE effects, *Chem. Commun.* 1 (2007) 70–72.
- [52] D. Wang, M.M.S. Lee, W.H. Xu, G.G. Shan, X.Y. Zheng, R.T.K. Kwok, J.W.Y. Lam, X.L. Hu, B.Z. Tang, Boosting non-radiative decay to do useful work: development of a multi-modality theranostic system from an AIEgen, *Angew. Chem.* 131 (2019) 5684–5688.
- [53] Y. Rachuri, B. Parmar, K.K. Bisht, ESuresh, Multiresponsive adenine-based luminescent Zn(II) coordination polymer for detection of Hg^{2+} and trinitrophenol in aqueous media, *Cryst. Growth Des.* 17 (2017) 1363–1372.
- [54] M.R. Han, W.X. Dong, S.S. Feng, L.P. Lu, Z.P. Li, An ultra-sensitive selective fluorescent sensor based on a 3D zinc-tetracarboxylic framework for the detection and enrichment of trace Cu^{2+} in aqueous media, *Dalton Trans.* 50 (2021) 4944–4951.
- [55] Y. Liu, C. Liu, X. Zhang, L. Liu, C. Ge, X. Zhuang, N.X. Zhang, Q. Yang, Y.Q. Huang, Z. Zhang, Highly selective and sensitive detection of Fe^{3+} , Al^{3+} and picric acid by a water-stable luminescent MOF, *J. Solid State Chem.* 272 (2019) 1–8.